Published in the Proceedings of the 2017 Annual International SFF Symposium

THE EFFECT OF POWDER ON COOLING RATE AND MELT POOL LENGTH MEASUREMENTS USING IN SITU THERMOGRAPHIC TECNIQUES

J. C. Heigel* and B. M. Lane*

*National Institute of Standards and Technology[1], Gaithersburg, MD 20899

Abstract

High-speed thermal cameras enable in situ measurement of the temperatures in and around melt pools generated during powder bed fusion processes. These measurements can be used to validate models, to monitor the process, and to understand the microstructure formed during the process. Unfortunately, pre-placed powder layers complicate the measurement due to spatter and irregular surfaces that impact emissivity. The objective of this work is to present high speed thermographic measurements of single and multiple scan tracks on substrates with and without pre-placed powder and to analyze and compare the impacts of powder on melt pool length and cooling rate measurements.

Introduction

Thermographic measurements of powder bed fusion (PBF) provide valuable insight into the process. The measurements can be used to study the process [1–3], to validate models [4], to better understand the material transformations that occur during the process [5–6], or to develop real-time monitoring and control techniques [7 - 11]. However, optical measurement of the surface temperature is challenging for a variety of reasons, such as the variable emissivity of the surface [12–13] and spatter that regularly occurs during the process [14]. While many studies have implemented thermographic techniques to measure the melt pool length and cooling rates during PBF processes, the impact of the process on the measurement and its error have not been well characterized.

Many of the challenges involved with thermography of PBF can be alleviated by removing the powder and studying the process while scanning on bare metal surfaces. Although this strategy removes the experiment from the actual process that consolidates layers of powder, it has two advantages. First, scans on bare surfaces are easier to measure, enabling the measurement itself to be studied. The second advantage is that the simplified process is easier to simulate and allows the modeler to validate the physics and material model without the powder, decreasing the number of variables in the model.

For instance, similar to other studies [1, 3, 4, 6, 7, 9–11], the earliest PBF thermography studies performed by the National Institute of Standards and Technology (NIST) were performed during the build of a small part [14–15]. Although informative, the chaotic nature of the spatter and the rough solidified surface made the process of quantifying the measurements difficult. Consequently, the experiments have been simplified by removing the powder so that better quality data could be acquired during single line

[1] Certain commercial equipment, instruments, or materials are identified in this paper in order to specify the experimental procedure adequately. Such identification is not intended to imply recommendation or endorsement by the National Institute of Standards and Technology, nor is it intended to imply that the materials or equipment identified are necessarily the best available for the purpose.

scans, enabling the melt pool length to be measured over the processing space [2] and to provide model validation data [5]. Now that the measurement process and thermal behavior of the material are better understood, powder can be re-introduced into the experiment so that its effect on the measurement and the process can be investigated.

This objective of this work is to present a preliminary investigation into the impact that powder has on thermographic measurements of melt pool length and cooling rate. Several cases are studied, two single line scans and two multiple scan tracks, half on a bare surface and the other half on a single layer of hand-spread powder. The acquired thermal images are qualitatively compared to understand spatter and the approximate length of the hot region as a function of line count. Radiant temperature profiles are extracted from these images and the cooling rate is calculated. Observations are made from these comparisons and their impact on the current work and on the future direction of the thermographic effort at NIST is discussed.

Experimental Method

The experiments consist of scanning single tracks and small areas using a commercial laser PBF machine and measuring the radiant temperature of the process using a high-speed thermal camera. The camera observes a 12 mm by 6 mm area in the build chamber through a custom fabricated door [2, 14]. The camera operates at a frame rate of 1800 Hz and an integration time of 40 µs, and the system is sensitive to wavelengths between 1350 nm and 1600 nm and can measure radiant temperature between 550 °C and 1038 °C. Although the camera does not directly measure the true temperature of the surface, the camera signal and surface temperature are related according to [16]:

$$S_{\text{meas}} = F(T_{\text{radiant}}) = \varepsilon \cdot F(T_{\text{true}}) + (1 - \varepsilon) \cdot F(T_{\text{environment}}) \quad (1)$$

where S_{meas} is the signal measured by the camera, $F(T_{\text{radiant}})$ is a calibration function to convert the signal measured by the camera to a black-body temperature, T_{true} is the actual temperature of the target surface, $T_{\text{environment}}$ is the temperature of the environment, and ε is the emissivity of the surface. When the emissivity of the surface is unknown, as in this study, the radiant temperature of the surface is reported.

Figure 1 presents the setup inside the build chamber. Figure 1A is a view through the viewport on the custom door of the rotary sample holder and five 25 mm square substrates (3 mm thick). Figure 1B shows a close-up of one of the samples after an area has been scanned.

Table 1 presents the four different cases studied in this work. Cases 1 and 2 produce single line scan tracks while Cases 3 and 4 scan a 5 mm x 4 mm area using multiple consecutive scans (39 in total, alternating direction). The scans are offset by 0.1 mm (hatch distance). Cases 1 and 3 are executed on bare substrates whereas Cases 2 and 4 are performed on a single hand-spread layer of powder (approximately 36 µm thick). In each case the nominal laser power is 195 W and the scan speed is 800 mm/s. In all cases, each scan track is 5 mm long.

Table 1 - The test cases investigated in the current work.

	Case 1	Case2	Case 3	Case 4
Number of scan tracks	1	1	39	39
Layer of powder?	No	Yes	No	Yes

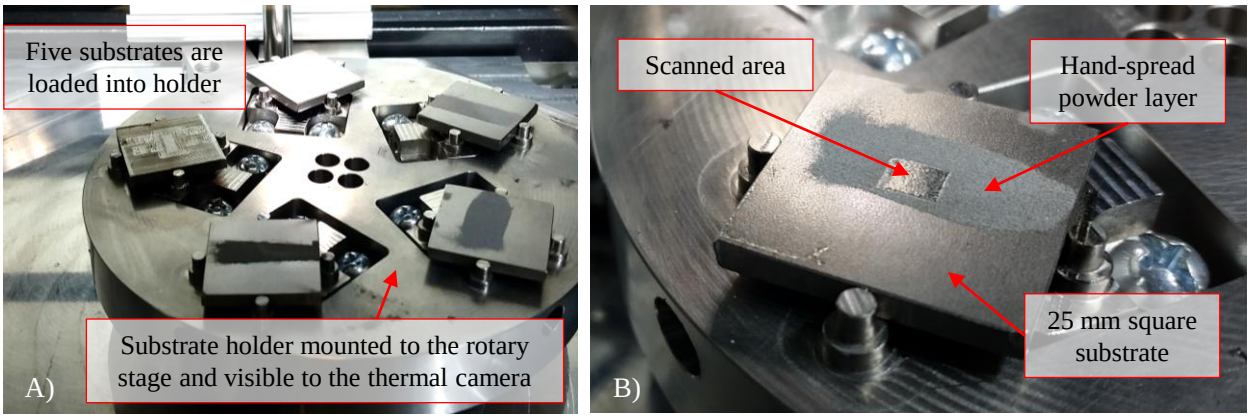

Figure 1 - Experiment setup inside the PBF build chamber. A) Image acquired through the viewport on the custom door showing the sample holder and small substrates. B) Close up of a substrate with a hand-spread powder layer after scanning an area (Case 4).

Results

Figure 2 presents select frames acquired during steady-state in Cases 1 and 2. As found in the prior study by the authors, steady-state occurs after the laser has traveled approximately 1.5 mm [2]. Case 1 appears to be more consistent and shorter than Case 2. The plume is visible following above the scan track, with a slight reflection of it below the track. In contrast, the Case 2 is far less consistent. A significant amount of spatter can be seen above and behind the track, making the images look far more

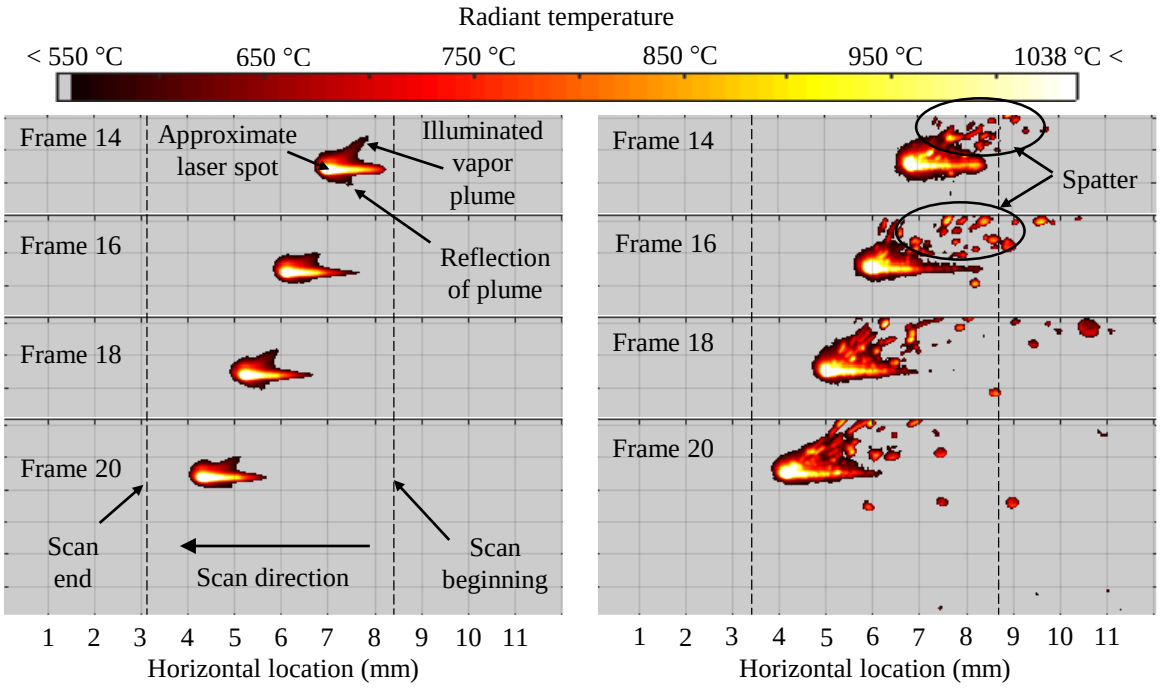

A) Case 1, single scan track on a bare plate

B) Case 2, single scan track on a layer of powder

Figure 2 - Select frames acquired using the thermal camera during steady state of the single scan tracks.

chaotic than the bare surface scans.

Select frames during the deposition of Cases 3 and 4 are shown in Figure 3. These frames are acquired immediately before the conclusions of their respective scan tracks. The length appears to increase as more lines are scanned and it seems that steady state is achieved shortly after the 7th scan track. In Case 4, which has a layer of powder, the amount of spatter is greater during the first scan track than in subsequent tracks.

Figure 4A presents the temperature profiles extracted along the scan track from each frame acquired during steady state in Cases 1 and 2. The melt pool length and the solidus-to-liquidus radiant temperature

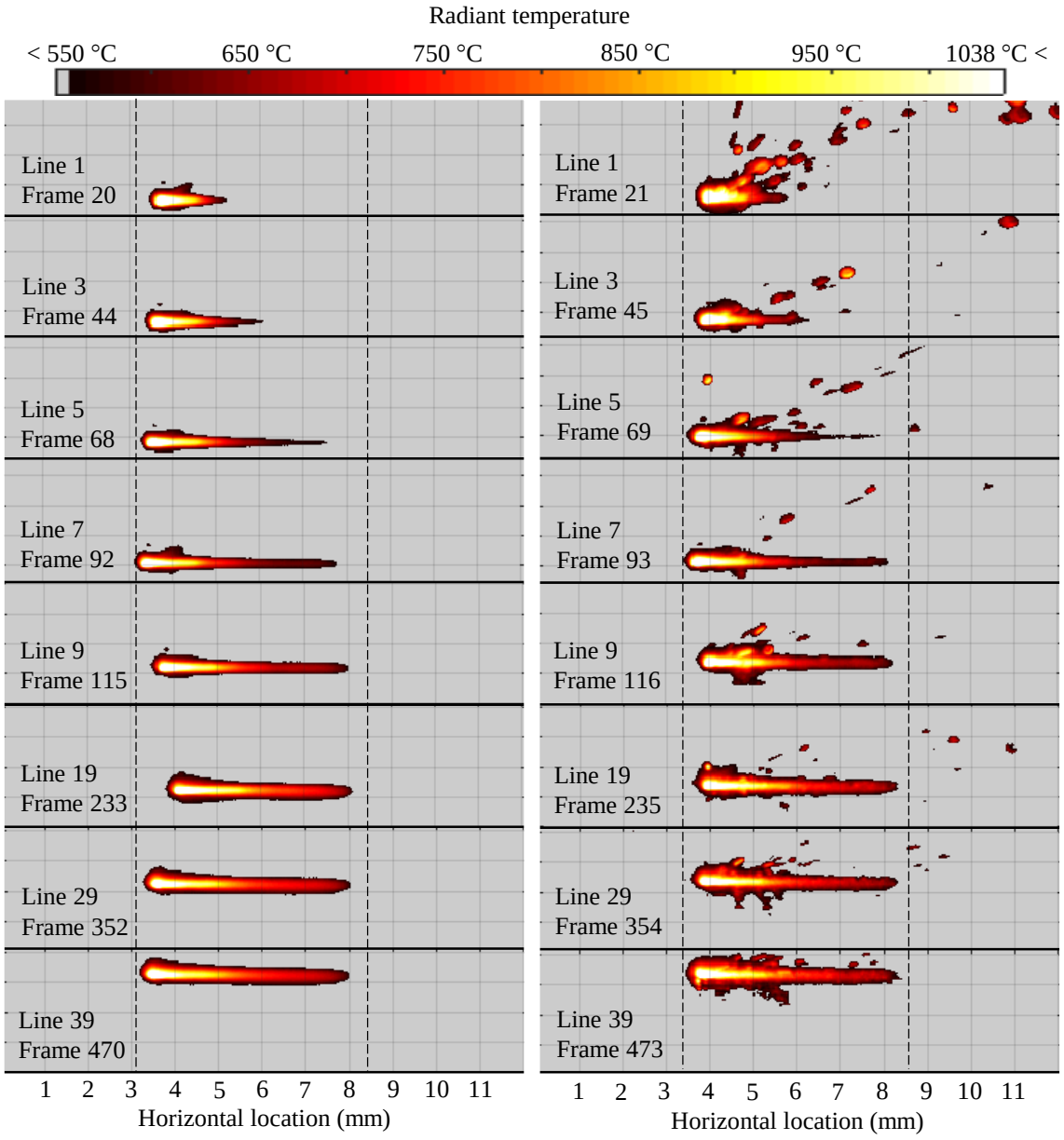

A) Case 3, multiple line scans on a bare plate B) Case 4, multiple line scans on a layer of powder

Figure 3 - Frames acquired immediately before the completion of select scan tracks during Cases 3 and 4.

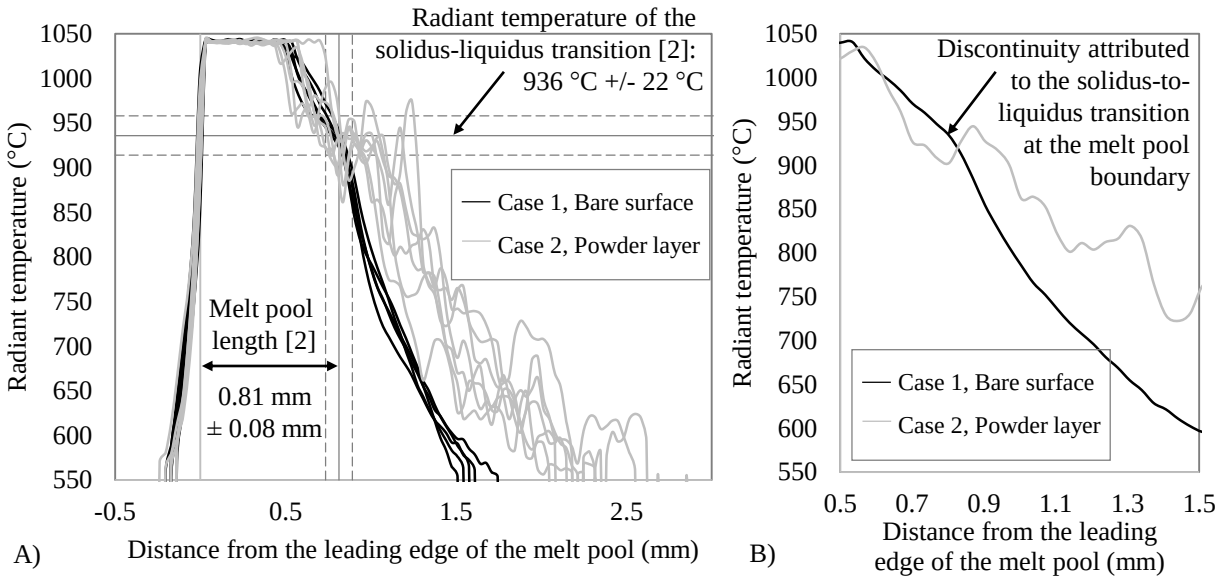

Figure 4 – The steady state radiant temperature profiles in Cases 1 and 2 (A). The vertical and horizontal lines indicate the melt pool length measurement and the solidus-to-liquidus radiant temperature [2]. For those values, one standard deviation is reported. B) an individual profile from each case to illustrate the discontinuity attributed to the solidus-to-liquidus transition.

found in the earlier study are included for comparison [2]. The gray horizontal lines indicate the radiant temperature of the solidus-to-liquidus transition while the vertical gray lines indicate the front and back of the melt pool, based on the length measured in the earlier study. These plots support the observations made of Figure 2. The bare surface scan in Case 1 produces consistent temperature profiles, whereas the Case 2 scan on a layer of powder produces profiles that have a significant amount of variation and have a greater radiant temperature. A closer investigation of these profiles suggests that, although the discontinuity associated with the solidus-to-liquidus transition cannot be detected in the powder case, it appears that the melt pool length is similar between the two cases, as illustrated with an example in Figure 4B.

Figure 5 presents temperature profiles of select scan tracks first shown in Figure 3. Once again, the profiles of the bare surface scan are smooth, whereas those of the powder layer scan have a significant amount of variation, though the variation is less as the scan line number increases. Although the discontinuity associated with the solidus-to-liquidus transition is imperceptible in the powder layer radiant temperature profiles due to this variability, the melt pool length can be measured by assuming the bare surface measurements in the previous study can be applied to the powder layer. If this assumption is valid, then in both cases the melt pool length nearly doubles in each case from the first line (approximate length of 0.76 mm) to the end of the 39th line (approximate length of 1.5 mm).

The rate at which the scan track cools from 900 °C to 700 °C (radiant temperature) is calculated using the following equation and the results are presented in Figure 5:

$$CR = \frac{200\ °C}{(p_{700\ °C} - p_{900\ °C})\,{}^{r}/_{v}} \tag{2}$$

where *CR* is the cooling rate in radiant temperature, *v* is the scan velocity (800 mm/s), *r* is the horizontal camera instantaneous field of view (0.036 mm per pixel), and *p* is the location (pixel) in the frame of interest where the radiant temperature profile equals 900 °C and 700 °C. The markers for Cases 1 and 2

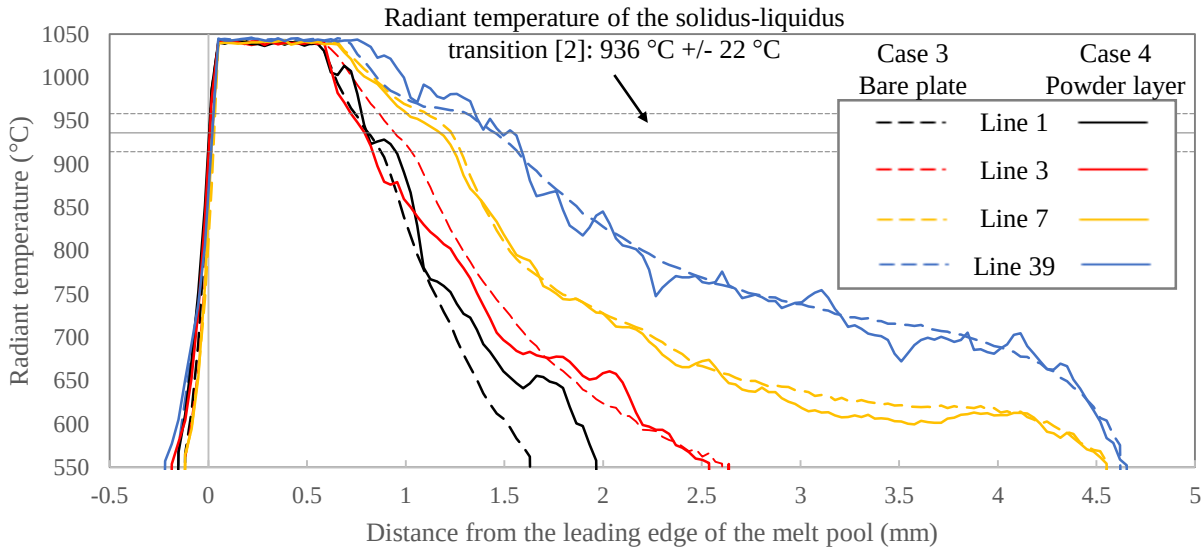

Figure 5 - The radiant temperature profile near the end of select scan track that were initially presented in Figure 3. The solid horizontal line indicates the mean solidus-to-liquidus transition temperature, while the dashed horizontal lines represent one standard deviation [2].

present the mean of calculations performed on all frames acquired during steady state. The standard deviation of those calculations (1σ) is reported in the text on the plot. The markers indicating Cases 3 and 4 represent the calculation from a single frame acquired at the end of each odd-numbered scan track. For each of the multiple scan track cases, the cooling rate decreases as the line count increases, reaching an apparent steady state value around the 20th line. The average and standard deviation (1σ) is calculated for the odd numbered scan tracks, from 21 to 39, and is reported on the figure. In both multi-line cases, the cooling rate decreases to values that are approximately 15 % to 20 % of the values measured in the single scan track cases. The standard deviation of the measured values also decreases by an order of magnitude or more from the single scan tracks to the steady state multiple track scans.

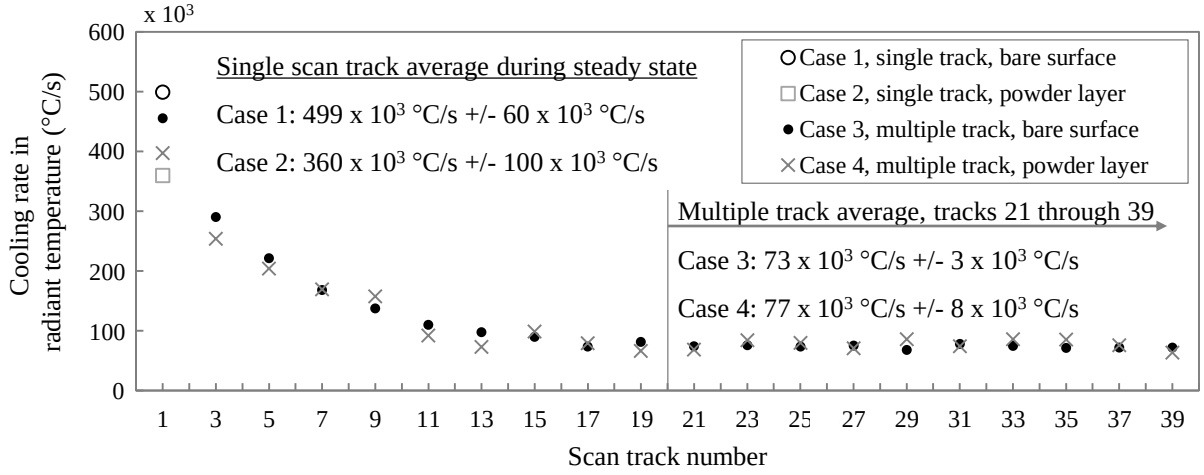

Figure 6 - The rate the material cools from 900 °C to 700 °C for each odd numbered scan track.

Discussion

The results presented in this work confirm that thermographic measurements of scan tracks on layers of powder are more complex than when the same scans are performed on bare surfaces. Scans on powder result in greater fluctuations along the temperature profile of the scan track behind the melt pool. Considering the camera system used in this study and its resolution, these fluctuations mask the discontinuity that is associated with the solidus-to-liquidus transition and could be detected in the bare surface scans. Since the discontinuity is regularly used to identify the melt pool boundary and measure the melt pool length, the melt pool length could not be measured without assuming the radiant temperature of the transition is similar in the bare surface and powder layer scans. Further work is required to confirm if this assumption is valid. In addition, the single scan tracks on a powder layer appear to be hotter than on bare surfaces, as demonstrated in Figure 4, and the cooling rate in radiant temperature is slower, as indicated in Figure 6. The hotter appearance and slower cooling rate in the radiant temperature scale could be attributed to two factors that require a more detailed analysis.

1) The powder layer effectively increases the absorption efficiency of the laser, leading to a greater amount of energy entering the part [17] and increasing the melt pool length and the residual temperature in the track.
2) The effective emissivity of the track is greater when created on a powder layer than on a bare surface, leading to an apparent hotter temperature in the radiant temperature scale even though the true temperature is equal to the bare surface scan. The effective emissivity could be elevated in the powder layer cases by:
    a. The rougher surface of the scan track [18].
    b. The elevated scan track (due to the solidified powder layer) changing the relative viewing angle, which has been shown to affect emissivity [12], [13].
    c. Reflections from the spatter on the scan track, increasing the signal measured by the camera according to Equation (1).

A more detailed investigation is required to understand the impact of each of these possible factors to understand whether powder does impact the melt pool length and the temperature in single track scans, or if it only appears to have an effect.

Analysis of the multiple scan track cases suggest that the temperature between the bare surface and powder layer scans are not as different as they appear in the single line cases. As the scan lines count increases, the temperature profiles of the two cases have better agreement, as shown in Figure 5. Furthermore, the variability appears to decrease, as does the spatter, after the first few lines, as indicated in Figure 5 and Figure 6. These observations suggest the following:

1) Spatter can have a significant impact on both the magnitude of the temperature profile and its variability.
2) The deposition of successive tracks, that are deposited moving away from the camera, has a different impact on effective emissivity than that of a single scan track.
3) The difference in energy absorption between scans on bare surface and single layers of powder is only significant for the first layer, since denudation draws powder into the track, exposing the bare surface for each successive track [19], [20].

Once again, a more detailed experiment must be designed to investigate these and other possibilities.

Conclusions

This work presented thermographic measurements acquired during the powder bed fusion process. Single and multiple scan tracks were executed on both bare surfaces and hand-spread powder layers. The results were compared to gain insight into the effect of powder on both the process and the measurement. Results indicate that the presence of powder increases the variability in the radiant temperature profiles behind the melt pool that that while the single scan tracks appear to be hotter in radiant temperature, it is unclear if the increase is due to differences in true temperature or the effective emissivity of the surface. The multiple scan track results indicate that the bare surface and powder layer scans are more similar as the number of scan lines increase. Future work will improve upon the experimental method and analysis to answer questions that could not be answered in this preliminary study.

References

[1] M. Doubenskaia, A. Domashenkov, and I. Smurov, "Study of the laser melting of pre-deposited intermetallic TiAl powder by comprehensive optical diagnostics," *Surface and Coatings Technology*, vol. 321, pp. 118–127, 2017.

[2] J. C. Heigel and B. Lane, "Measurement of the Melt Pool Length During Single Scan Tracks in a Commercial Laser Powder Bed Fusion Process," in *Proceedings of the ASME 2017 12th International Manufacturing Science and Engineering Conference (MSEC 2017)*, Los Angeles, CA, 2017, vol. 12.

[3] E. Rodriguez, J. Mireles, C. A. Terrazas, D. Espalin, M. A. Perez, and R. B. Wicker, "Approximation of absolute surface temperature measurements of powder bed fusion additive manufacturing technology using in situ infrared thermography," *Additive Manufacturing*, vol. 5, pp. 31–39, 2015.

[4] S. Price, B. Cheng, J. Lydon, K. Cooper, and K. Chou, "On Process Temperature in Powder-Bed Electron Beam Additive Manufacturing: Process Parameter Effects," *Journal of Manufacturing Science and Engineering*, vol. 136, no. 6, p. 061019, 2014.

[5] T. Keller *et al.*, "Application of finite element, phase-field, and calphad-based methods to additive manufacturing of Ni-based superalloys," *Acta Materialia*, 2017.

[6] I. Yadroitsev, P. Krakhmalev, and I. Yadroitsava, "Selective laser melting of Ti6Al4V alloy for biomedical applications: Temperature monitoring and microstructural evolution," *Journal of Alloys and Compounds*, vol. 583, pp. 404–409, 2014.

[7] J.-P. Kruth, P. Mercelis, J. Van Vaerenbergh, and T. Craeghs, "Feedback control of selective laser melting," in *Proceedings of the 3rd International Conference on Advanced Research in Virtual and Rapid Prototyping*, 2007, pp. 521–527.

[8] P. Lott, H. Schleifenbaum, W. Meiners, K. Wissenbach, C. Hinke, and J. Bültmann, "Design of an optical system for the in situ process monitoring of selective laser melting (SLM)," *Physics Procedia*, vol. 12, pp. 683–690, 2011.

[9] M. Doubenskaia, M. Pavlov, S. Grigoriev, E. Tikhonova, and I. Smurov, "Comprehensive optical monitoring of selective laser melting," *Journal of Laser Micro Nanoengineering*, vol. 7, no. 3, pp. 236–243, 2012.

[10] H. Krauss, C. Eschey, and M. Zaeh, "Thermography for monitoring the selective laser melting process," presented at the Proceedings of the Solid Freeform Fabrication Symposium, 2012.

[11] J. Raplee *et al.*, "Thermographic Microstructure Monitoring in Electron Beam Additive Manufacturing," *Scientific Reports*, vol. 7, p. 43554, 2017.

[12] J. Heigel, B. Lane, and S. Moylan, "Variation of Emittivity with Powder Bed Fusion Build Parameters," presented at the Proceedings of the 2016 Annual International SFF Symposium, 2016.

[13] L. del Campo *et al.*, "Emissivity measurements on aeronautical alloys," *Journal of Alloys and Compounds*, vol. 489, no. 2, pp. 482–487, Jan. 2010.

[14] B. Lane *et al.*, "Thermographic measurements of the commercial laser powder bed fusion process at NIST," *Rapid prototyping journal*, vol. 22, no. 5, pp. 778–787, 2016.
[15] B. Lane, E. Whitenton, and S. Moylan, "Multiple sensor detection of process phenomena in laser powder bed fusion," presented at the SPIE Commercial+ Scientific Sensing and Imaging, 2016, pp. 986104–986104.
[16] B. Lane, E. Whitenton, V. Madhavan, and A. Donmez, "Uncertainty of temperature measurements by infrared thermography for metal cutting applications," *Metrologia*, vol. 50, no. 6, p. 637, 2013.
[17] R. W. McVey, R. M. Melnychuk, J. A. Todd, and R. P. Martukanitz, "Absorption of laser irradiation in a porous powder layer," *Journal of Laser Applications*, vol. 19, no. 4, pp. 214–224, Nov. 2007.
[18] G. Strano, L. Hao, R. M. Everson, and K. E. Evans, "Surface roughness analysis, modelling and prediction in selective laser melting," *Journal of Materials Processing Technology*, vol. 213, no. 4, pp. 589–597, 2013.
[19] I. Yadroitsev, P. Bertrand, and I. Smurov, "Parametric analysis of the selective laser melting process," *Applied surface science*, vol. 253, no. 19, pp. 8064–8069, 2007.
[20] M. J. Matthews, G. Guss, S. A. Khairallah, A. M. Rubenchik, P. J. Depond, and W. E. King, "Denudation of metal powder layers in laser powder bed fusion processes," *Acta Materialia*, vol. 114, pp. 33–42, 2016.